Journal of Materials Chemistry A

Unraveling the Role of Structural Water in Bilayer V2O5 during Zn2+-Intercalation: Insights from DFT Calculations

Journal:	*Journal of Materials Chemistry A*
Manuscript ID	TA-ART-12-2018-012014.R1
Article Type:	Paper
Date Submitted by the Author:	20-Jan-2019
Complete List of Authors:	Wu, Tao; University of South Carolina, Mechanical Engineering Zhu, Kaiyue; University of South Carolina, Mechanical Engineering Qin, Changyong; Benedict College, Biology and Chemistry Huang, Kevin; University of South Carolina, Mechanical Engineering

Unraveling the Role of Structural Water in Bilayer V_2O_5 during Zn^{2+}-Intercalation: Insights from DFT Calculations

Tao Wu[a], Kaiyue Zhu[a], Changyong Qin[b] and Kevin Huang*[,a]

[a] Department of Mechanical Engineering, University of South Carolina, Columbia, SC 29208

[b] Department of Chemistry and Biology, Benedict College, Columbia, SC 29204

† Electronic supplementary information (ESI) available. See DOI: XXXXXX.

*Corresponding author: huang46@cec.sc.edu

Abstract

Bilayer structured $V_2O_5 \cdot nH_2O$ has recently been studied as a promising cathode material for aqueous Zn^{2+}-batteries (ZIBs) due to its ion-intercalatable layer structure and high theoretical capacity. An interesting observation in this system is the beneficial effect of structural water (nH_2O) on the electrochemical performance, but a fundamental understanding on the underlying reason is still lacking. Herein, we report a systematic density functional theory investigation into why and how structural water in the bilayer $V_2O_5 \cdot nH_2O$ affects structure, voltage, migration barrier and capacity during Zn^{2+}-intercalation process. The results suggest that the structural water acts as extra host sites to accept electrons from Zn, resulting in a stronger ionization of Zn^{2+} than dry V_2O_5 and thus higher open-circuit voltage (OCV). It is also found that structural water creates a smoother electrostatic environment between V_2O_5 sheets for easy Zn^{2+} diffusion. Benefited from such a combined "charge shielding" and "O in H_2O interaction with Zn^{2+}" effect, $V_2O_5 \cdot H_2O$ and $V_2O_5 \cdot 1.75H_2O$ exhibit lower Zn^{2+}-diffusion barrier and higher OCV than non-hydrated V_2O_5. Overall, this DFT study reveals mechanistic insights into the importance of structural water in promoting Zn^{2+}-intercalation process in bilayer V_2O_5.

Introduction

A deeper penetration of renewable energy into existing electrical grids calls for the development of large-scale and cost-effective energy storage technologies such as rechargeable batteries.[1-3] The benchmark non-aqueous based Li-ion battery (LIB) technology is not suitable for the application because of the concerns in safety, cost and sustainability.[4-7] Other non-aqueous based Na-ion and K-ion batteries are sustainable for large-scale applications from a resource perspective, but their safety remains a major concern due to the use of flammable organic electrolytes.[8-12] A potential solution to overcome the safety and cost barriers is to switch the liquid electrolyte from organic to aqueous solvents. There are several advantages that can be gained from this switch: better safety, lower cost, higher ionic conductivity (~1 *vs* 10^{-2}-10^{-3} S cm^{-1}),[13] and easier ambient manufacturing.[14-18] But the disadvantage is lower operating voltage (~1 *vs* 3 V), which may result in lower energy capacity (J/kg or J/L). This disadvantage may be critical for portable electronics applications, but not necessarily for large-scale applications since safety and cost are the two most crucial criteria.

Attracted by the above unique advantages for potential large-scale energy storage applications, a range of aqueous-based battery chemistries based on alkali metal cations (e.g., Na^+ and K^+)[19, 20] and multivalent cations (e.g., Mg^{2+}, Ca^{2+}, Zn^{2+} and Al^{3+}) have been explored in recent years.[21] For the multivalent cation chemistry, higher volumetric charge capacity and energy density are also expected because of the nature of multi-electron transfers.[11, 22] Among all aqueous-based rechargeable batteries, Zn-ion batteries (ZIBs) stand out to be the most promising candidate.[23] First, Zn is a low-cost, nontoxic and earth-abundant material. Second, Zn has a high theoretical

volumetric charge capacity (5,854 *vs* 2,042 mA h cm^{-3} for Li), [24] low redox potential (-0.76 V *vs* SHE) and rather reversible Zn/Zn^{2+} redox kinetics. [25] For these reasons, Zn has been a benchmark anode material for primary Zn-MnO_2 battery and secondary Zn-Ni and Zn-Mn batteries.[26-28] However, its low reduction potential presents a challenge to identify a suitable Zn^{2+} host cathode material with a high oxidation potential, into which Zn^{2+} can be intercalated. Therefore, a key development to the next-gen ZIBs is the discovery of new cathodes that can host Zn^{2+} with reversibility.

Promising cathode materials of ZIBs are so far primarily found in MnO_x, VO_x and Prussian blue analogues, all of which have a strong oxidation potential to accept electrons from Zn.[11] One unique phenomenon observed in VO_x cathode is that the presence of structural water can facilitate Zn^{2+} intercalation kinetics. For example, Kundu *et al.* demonstrated that the structural water in $Zn_{0.25}V_2O_5 \cdot nH_2O$ plays a role in facilitating expansion and contraction of layer-layer galleries to allow a reversible Zn^{2+} intercalation/extraction, thus giving a good kinetics and rate performance.[29] Yan *et. al* experimentally showed that the structural water in V_2O_5 can work as a "charge screen" to decrease electrostatic interactions between the solvated Zn^{2+} and V_2O_5 framework, thus allowing a faster Zn^{2+}-diffusion.[30] Kundu *et al.* further showed a lower charge transfer resistance and activation energy for aqueous systems than non-aqueous counterparts, and emphasized the importance of de-solvation of Zn^{2+} in Zn^{2+}-intercalation into the host $V_3O_7 \cdot nH_2O$.[24] Apart from that, some previous studies also suggest the solvating H_2O can work as a charge shield for the metal ions, reducing their effective charges and hence their interactions with the host frameworks in intercalation process.[31-34]

It is evident from these early studies that the structural water in VO_x plays a promotional role in the Zn^{2+}-intercalation kinetics. However, the detailed fundamental mechanisms elucidating this

role have not been well understood. Herein we report a systematic density functional theory (DFT) investigation into the role of structural water in Zn^{2+}-intercalation into a model bilayer V_2O_5. The DFT calculations are performed to answer the questions such as how structural water (in the case of $V_2O_5{\cdot}H_2O$ and $V_2O_5{\cdot}1.75H_2O$) affects crystal structure, electronic structure, Zn^{2+}-migration barrier, voltage and capacity. We also show how structural water shields charges from V_2O_5 sheet and rebuilds a smoother electrostatic environment to allow easier Zn^{2+}-diffusion.

Computational Method

First-principles computational methods, particularly density functional theory (DFT), presents advantages to understand the mechanisms at atomic/molecular scales, since it can isolate distinct physical/chemical phenomena and quantitatively assess their thermodynamics and kinetics. This capability is critically important in identification of specific structural and chemical features, such as Zn^{2+}-intercalation process in ZIBs.

Herein, we apply DFT method to calculate the ground states of bilayer V_2O_5, $V_2O_5{\cdot}H_2O$ and $V_2O_5{\cdot}1.75H_2O$ in the pristine and Zn^{2+}-intercalated states. All calculations were performed by Perdew-Burke-Ernzerhof (PBE) generalized gradient approximation (GGA) exchange-correlation implemented in the Vienna ab Initio Simulation Package (VASP).[35-37] The projector augmented wave (PAW) method was used to describe the interaction between core electrons and valence electrons.[38-39] Valence configurations include the H ($1s^1$), O ($2s^2 2p^4$), V ($3p^6 3d^4 4s^1$) and Zn ($3d^{10} 4p^2$) states. All calculations were run with a cutoff energy of 400 eV, Gaussian smearing and normal precision. For thermodynamic calculations such as lattice parameters and voltage, we employed the DFT+U formalism of Anisimov *et al.* to account for strong on-site Coulombic interactions of the V 3d-electrons, with a specific on-site potential of U = 3.25 eV.[40] To explicitly account for van der Waals' interactions between layers and structural water, van der waals-

corrected D2 method of Grimme was used for all calculations.[41] The lattice constants and atomic positions were both fully relaxed until a maximum energy difference and residual force on atoms converge were reached at 10^{-4} eV and 0.05 eV/Å, respectively. The Brillouin zone was first sampled with 2×8×2 to predict the lattice constants for the unit cell of bilayer V_2O_5. Then, large supercells (1×2×1) of bilayer V_2O_5 were used to describe the intercalation of Zn^{2+} at different concentrations, and the corresponding Monkhorst-Pack grids were 2×4×2. In this way, metal-metal interactions can be neglected and the interaction between inserted Zn^{2+} and bilayered V_2O_5-host can be studied.

To model ionic diffusion in the selected host structure, we employed climbing-image nudged elastic band (CI-NEB) method to couple with density functional theory (DFT).[42] We elected to use DFT instead of DFT+U because an early first-principles calculations of multivalent-ion migration in oxide spinels has shown a pronounced metastability of electronic states along the ion migration path with U, resulting in a poor computational convergence; [43] the study also reported that no significant improvements in the diffusion barriers were found using DFT+U calculations.[43-44] The convergence threshold of the total energy was set to 1×10^{-4} eV, and a tolerance of 0.1 eV/A for the forces was used in the CI-NEB procedure. A total of eight images were interpolated between the initial and final relaxed structures in each case. To avoid spurious interactions, 1×2×1 supercells were used for barrier calculations.

Results and discussion

Crystal Structure

The bilayer V_2O_5 polymorph crystallizes with a space group symmetry of C2/m and has two distinct octahedral units, which share edges along the ***a*** and ***b*** axes to form infinite sheets. The periodic crystal structure is built from repeating layered units along the ***c***-axis bonded by weak van

der Waals forces, which is favorable to guest ion intercalation. However, there are so far no reported studies in which a bilayer V_2O_5 gel was created in absence of water.[45] This suggests that structural water is crucial in stabilizing the bilayers. Thus, for our DFT calculations we include 1.0 H_2O and 1.75 H_2O between the two V_2O_5 sheets to study their effects on Zn^{2+} intercalation. It should be noted that the structural water molecules can take a variety of positions within the bilayer V_2O_5, which can lead to various local minima configurations. Since it is too complicated to explore all of them, we only choose in DFT calculations relevant water configurations with more hydrogen bonds that will lead to lower total system energy. The optimized (1×2×1) supercell of these three structures (each structure has 16 V-atoms) is illustrated in Fig. 1. With water introduced into V_2O_5 bilayers, the two V_2O_5 sheets will suffer from little translation and distortion, leading to ***a*** and ***c*** axes out of vertical direction, in reference to water-free bilayer V_2O_5.

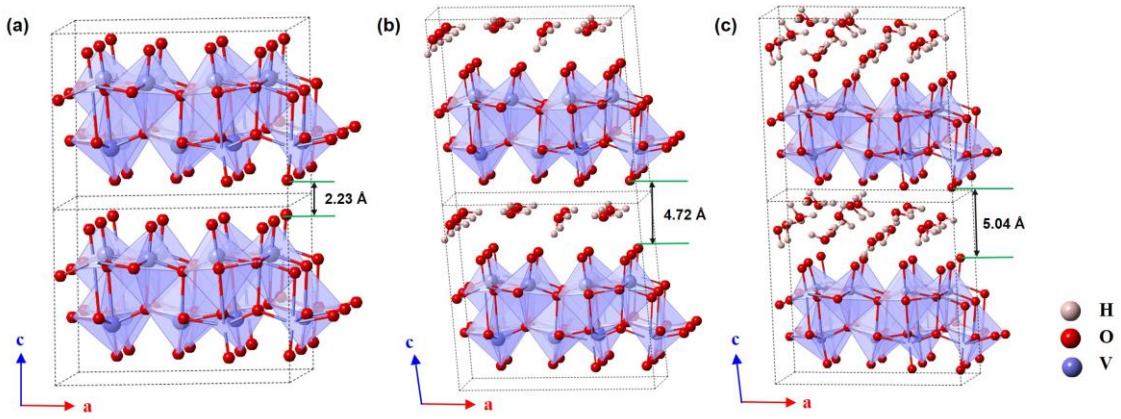

Fig. 1 Optimized (1×2×1) supercell of bilayer (a) V_2O_5, (b) $V_2O_5{\cdot}H_2O$ and (c) $V_2O_5{\cdot}1.75H_2O$. The distance between layers for three structures is also given in the figure.

Table 1 The lattice parameters for compound V_2O_5, $V_2O_5{\cdot}H_2O$ and $V_2O_5{\cdot}1.75H_2O$.

Compound	a (Å)	b (Å)	c (Å)
V_2O_5	11.58	3.65	8.59
$V_2O_5{\cdot}H_2O$	11.54	3.63	10.98

$V_2O_5 \cdot 1.75H_2O$	11.63	3.61	11.35
$V_2O_5 \cdot nH_2O$ (exp.)[46]	11.72	3.57	11.52

The calculated lattice parameters for bilayer V_2O_5, $V_2O_5 \cdot H_2O$ and $V_2O_5 \cdot 1.75H_2O$ are summarized in Table 1. We notice that lattice parameters of ***a*** and ***b*** axes are similar for the three models, but the length of ***c*** axe monotonously increase from 8.59 to 11.35 Å with the introduction of water. It also corresponds to the increased gallery spacing between the two V_2O_5 sheets in the structures shown in Fig. 1. The distance between the two V_2O_5 sheets for bilayer V_2O_5, $V_2O_5 \cdot H_2O$ and $V_2O_5 \cdot 1.75H_2O$ are 2.23, 4.72 and 5.04 Å, respectively. Since the number of structural water determined by experiment is ~1.8, we can directly compare the modeled lattice parameters of $V_2O_5 \cdot 1.75H_2O$ to the experimental results. The optimized lattice parameters of $V_2O_5 \cdot 1.75H_2O$ is a=11.63 Å, b= 3.61 Å, c= 11.35 Å, which agrees reasonably well with the experimental values: a=11.72 Å, b= 3.57 Å, c= 11.52 Å.[46] This agreement confirms that our supercells built for DFT calculations are appropriate.

In addition, the formation energies for H_2O in hydrated V_2O_5 are calculated by:

$$\Delta E_f = \frac{E(V_2O_5 \cdot xH_2O) - E(V_2O_5) - xE(H_2O)}{x} \quad (1)$$

where $E(V_2O_5 \cdot xH_2O)$ is the total energy of $V_2O_5 \cdot H_2O$ or $V_2O_5 \cdot 1.75\ H_2O$. $E(V_2O_5)$ and $E(H_2O)$ are the total energy of bilayer V_2O_5 and gas phase H_2O. *x* is the number of H_2O molecules in the lattice. The calculated formation energies of H_2O in $V_2O_5 \cdot H_2O$ and $V_2O_5 \cdot 1.75\ H_2O$ are -0.24 eV and -0.15 eV, respectively. The negative formation energy implies that the structural H_2O in bilayer V_2O_5 is thermodynamically stable.

Structural Configurations for Zn^{2+} Intercalation

To obtain the structural configurations for Zn^{2+}-intercalation with a local minimum, we have tried many possible intercalation configurations (see Fig S1, S2 and S3†) and the final optimized structural configurations for intercalating 1, 2, 4, and 8 Zn^{2+} are shown in Fig. 2. We can conclude from this calculation that there are at most eight intercalatable Zn^{2+} for all supercells due to limited host sites in the gallery. As shown in Fig. 2a1~a4, Zn^{2+} are in the gallery and connected with V_2O_5 sheets in dry V_2O_5. This arrangement implies that Zn^{2+} can simultaneously interact with the two V_2O_5 sheets. However, for $V_2O_5{\cdot}H_2O$, Zn^{2+} can only interact with one V_2O_5 sheet (top or below). This is because the H_2O in $V_2O_5{\cdot}H_2O$ enlarges the gallery spacing and shields the charge between $Zn^{2+}$and the other V_2O_5 sheet. The only exception is the structure shown in Fig. 2b2 with two Zn^{2+} intercalated, where decrease of gallery spacing and reorganization of H_2O are observed. For $V_2O_5{\cdot}1.75H_2O$ with a larger gallery spacing and two layers of water, the electrostatic interactions between Zn^{2+} and the two V_2O_5 sheets are effectively shielded.

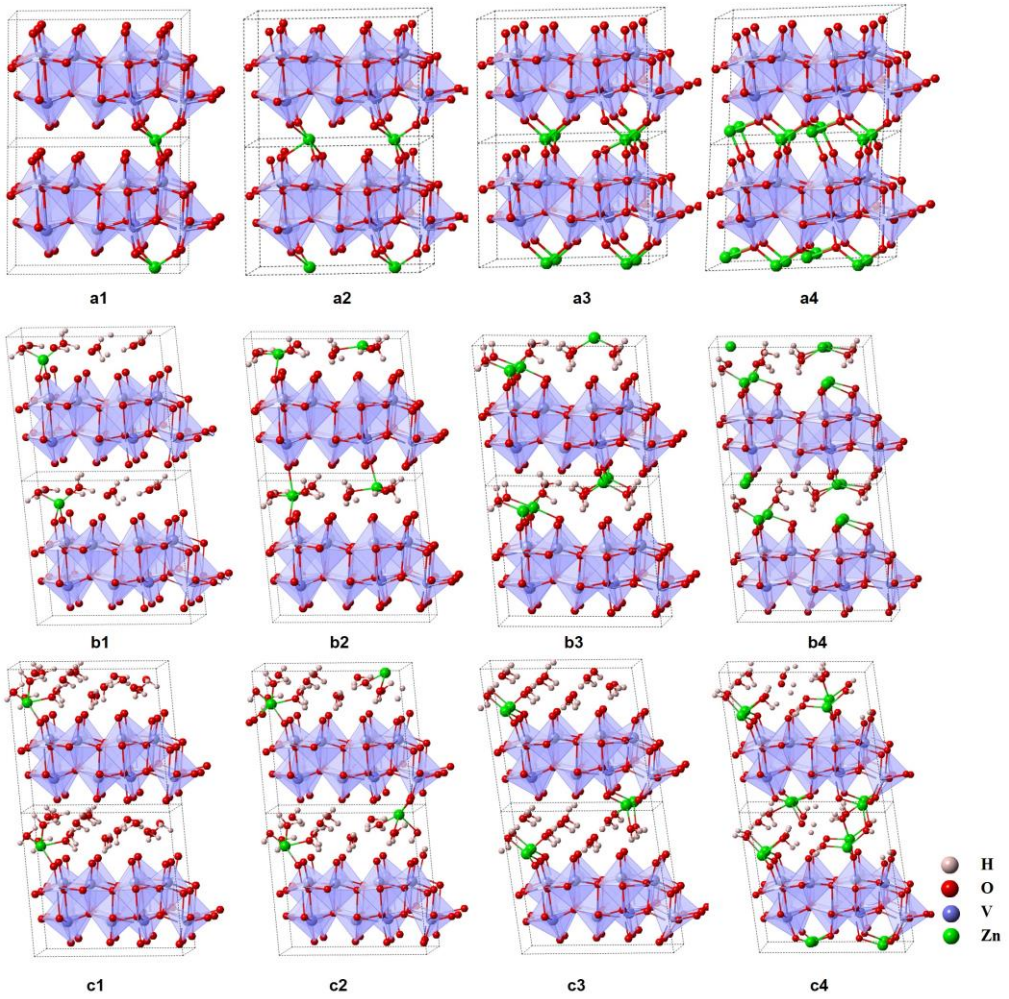

Fig. 2 The structural configurations for Zn^{2+} intercalation in (1×2×1) supercell of (a) V_2O_5, (b) $V_2O_5{\cdot}H_2O$ and (c) $V_2O_5{\cdot}1.75H_2O$ with different Zn^{2+} concentrations.

Although the structural water shields the interaction between Zn^{2+} and V_2O_5 sheets, and decreases their formation energy, the O in H_2O can also interact with Zn^{2+} in theory. Thus, the net effect of structural water may not necessarily decrease the formation energy between Zn^{2+} and V_2O_5, which will be discussed below in details. Another fact worth noting is the water dissociation with Zn^{2+} intercalation at high Zn^{2+} concentrations, see Fig. 2c4, into H^+ and OH^- in the gallery. This insight is consistent with the experimental observation of solvated protons (H_3O^+) by infrared spectroscopy in $V_2O_5{\cdot}nH_2O$.[47]

After discussing possible Zn^{2+}-intercalation sites and the coordination environment around Zn^{2+}, we now look into the volumetric change induced by Zn^{2+}-intercalation, which is an important practical consideration as a large volume change can lead to electromechanical degradation and loss of capacity.[48] Fig. 3a and 3b show the absolute volumetric change and relative volumetric change for V_2O_5, $V_2O_5 \cdot H_2O$ and $V_2O_5 \cdot 1.75H_2O$ at different Zn^{2+}-intercalation states, respectively. We observe that Zn^{2+}-intercalation in all three structures initially leads to a lattice contraction, then expansion at higher Zn^{2+} concentration. This is because there is enough space for Zn^{2+}-intercalation at low concentrations, the strong electrostatic attractions between Zn^{2+} and V_2O_5-sheets leads to the reduction of gallery spacing and lattice contraction. At higher Zn^{2+}-concentrations, the host must make more spaces for extra volumes to counteract the strong electrostatic interactions between cations, thus offsetting the lattice contraction. In addition, the relative volumetric change of dry V_2O_5 is small (< 2.5%) when the number of Zn^{2+} intercalated is < 4. However, this change will exceed 15% when the number of Zn^{2+} intercalated is 8. This result suggests that bilayer V_2O_5 in absence of water is stable at low concentrations of Zn^{2+} but becomes unstable at high Zn^{2+} concentrations. For $V_2O_5 \cdot H_2O$ and $V_2O_5 \cdot 1.75H_2O$, the volume changes are less than 10%, suggesting that these materials are more stable for practical applications.

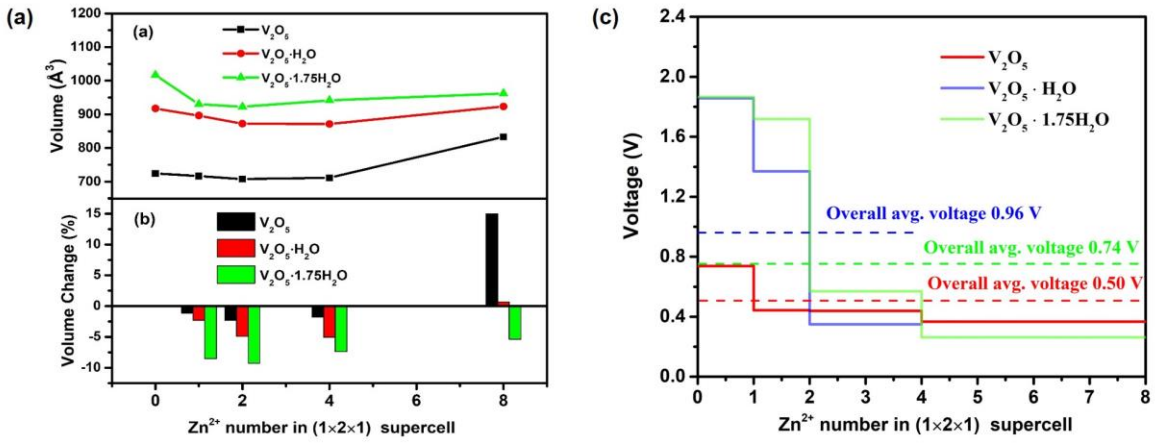

Fig. 3 (a) The absolute volumetric change and (b) relative volumetric change for V_2O_5, $V_2O_5{\cdot}H_2O$ and $V_2O_5{\cdot}1.75H_2O$ at different numbers of Zn^{2+} intercalated. (c) The average voltage for V_2O_5, $V_2O_5{\cdot}H_2O$ and $V_2O_5{\cdot}1.75H_2O$ at different states of Zn^{2+} intercalation.

Zn^{2+}-Intercalation Model

The model for Zn^{2+} intercalation into the layers between V_2O_5 follows that Zn^{2+} intercalate into each layer simultaneously with the same concentration. This is different from the conventional Li^+ intercalation into graphite, which follows stages.[49, 50] In this "staging" model, due to the small interlayer spacing within graphite, the intercalant must overcome the cohesive van-der-Waals energy between two adjacent graphene layers; the electrostatic repulsion between different intercalant layers as well as an intralayer attraction between intercalant atoms induces further intercalation within the same layer, contrary to further intercalation into another unoccupied layer. These effects combined are thought to be responsible for the "staging" mechanism. Experimentally, this has been confirmed by the appearance of new characteristic peaks from operando X-ray diffraction patterns for graphite.[49, 51]

For the cathode materials $V_2O_5{\cdot}H_2O$ and $V_2O_5{\cdot}1.75\ H_2O$ studied here, however, the interlayer spacing (4.72 Å for $V_2O_5{\cdot}H_2O$ and 5.04 Å for $V_2O_5{\cdot}1.75\ H_2O$) is large enough to accommodate Zn^{2+} (radius of Zn^{2+} is 0.74 Å), which ensures a small change of interlayer spacing during Zn^{2+} intercalation. Therefore, it is reasonable to assume that Zn^{2+} intercalate into each layer simultaneously. This has also been confirmed by the operando X-ray diffraction of $Zn_{0.25}V_2O_5$ during Zn-ions intercalation.[29] Unlike graphite, there is no appearance of new characteristic peaks for the cathode material during Zn^{2+} intercalation, which suggests that the mechanism of Zn^{2+} intercalation into $V_2O_5{\cdot}1.75\ H_2O$ layers is not the same as graphite.

Average Voltage vs the State of Zn^{2+}-Intercalation

Operating voltage is an important criterion to evaluate the electrochemical performance of V_2O_5, $V_2O_5 \cdot H_2O$ and $V_2O_5 \cdot 1.75H_2O$ as cathode materials for ZIBs. With a Zn metal as the anode, the average voltages of Zn^{2+} intercalation into a cathode can be calculated by:

$$V = -\frac{E^{cathode}(x_2) - E^{cathode}(x_1) - E(Zn)}{(x_2 - x_1)e}, x_2 > x_1 \quad (2)$$

where $E^{cathode}$ is the Gibbs free energy of the compound approximated by the total energy calculated by DFT at 0 K; x_1 and x_2 are the numbers of Zn^{2+} intercalated, respectively; E(Zn) is the Gibbs free energy per atom of the Zn anode (hcp); e represents the electronic charge. At $x_1 = 0$ and $x_2 = 1$, the open circuit voltage (OCV), a thermodynamic quantity of cathode, can be obtained. The average OCVs calculated are 0.74, 1.85 and 1.86 V for bilayer dry V_2O_5, $V_2O_5 \cdot H_2O$, $V_2O_5 \cdot 1.75H_2O$, respectively. Evidently, the OCV is increased by structural water in V_2O_5 layers.

It should be pointed out that the calculated OCV for $V_2O_5 \cdot 1.75H_2O$ is higher than the experimental value (~1.3 V).[29] We speculate that the functional including the van de waals interaction may be the reason.[52] The calculated OCVs by different functional are compared in Fig. S5 of the ESI†. On the other hand, the equilibrium potential measured between a real electrolyte and electrode could also be underestimated. Since DFT-D2 method produces the closest lattice parameter (see Table S1 in the ESI) to the experimental values (more reliably obtained), we believe that DFT-D2 is a more appropriate method than other methods to be used in the calculations. Nevertheless, the slight difference in OCV should not affect the discussion here of average voltage trending. The calculated voltages for V_2O_5, $V_2O_5 \cdot H_2O$ and $V_2O_5 \cdot 1.75H_2O$ are depicted in Fig. 3c, where the average voltages are continuously shown to decrease with the state of Zn^{2+}-intercalation for all the structures. But the decrease of average voltage for $V_2O_5 \cdot 1.75H_2O$ is less than that for $V_2O_5 \cdot H_2O$. Furthermore, there are at most 4 intercalatable Zn^{2+} in $V_2O_5 \cdot H_2O$ because the formation energy

becomes positive at eight Zn^{2+}, which implies a lower capacity for $V_2O_5 \cdot H_2O$. We also calculated overall average voltage over an entire discharge process. The overall average voltage of $V_2O_5 \cdot H_2O$ is the highest among the three structures, which reaches 0.96 V. Due to the limited discharge capacity (intercalating only 4 Zn^{2+}) in $V_2O_5 \cdot H_2O$, there is no reason to compare it further with others. However, the discharge process of V_2O_5 and $V_2O_5 \cdot 1.75H_2O$ are complete. The overall average voltage of $V_2O_5 \cdot 1.75H_2O$ is 0.74 V, which is consistent with the experimental 0.71 V given other losses, and higher than 0.50 V of pure V_2O_5.[29]

Electronic Structure

To further understand the water effect on the average voltage, electronic structure calculations have been performed. Fig. 4a-c illustrate the corresponding density of states (DOS) of V_2O_5, $V_2O_5 \cdot H_2O$, $V_2O_5 \cdot 1.75H_2O$ in pristine and Zn^{2+}-intercalated states. For V_2O_5, the valence and conduction bands are mainly contributed from O and V ions in the V_2O_5 layer. However, for $V_2O_5 \cdot H_2O$ and $V_2O_5 \cdot 1.75H_2O$, the valence and conduction bands are mainly contributed from O-ions in H_2O, which suggests O-ions in H_2O also participate in receiving electrons from Zn.[53] As depicted in the figure, Zn^{2+}-intercalation shifts DOS to lower energy regime, implying electron transfer of Zn to the conduction band. The shift of DOS further pushes the Fermi level of all Zn^{2+}-intercalated structures through the conduction band, resulting in a higher electrical conductivity than without Zn^{2+}. Furthermore, the DOS of Zn is very small and flat, implying that electrons from Zn distribute over a large energy landscape and delocalized. Therefore, a strong hybridization between Zn and O ions is almost unobservable.

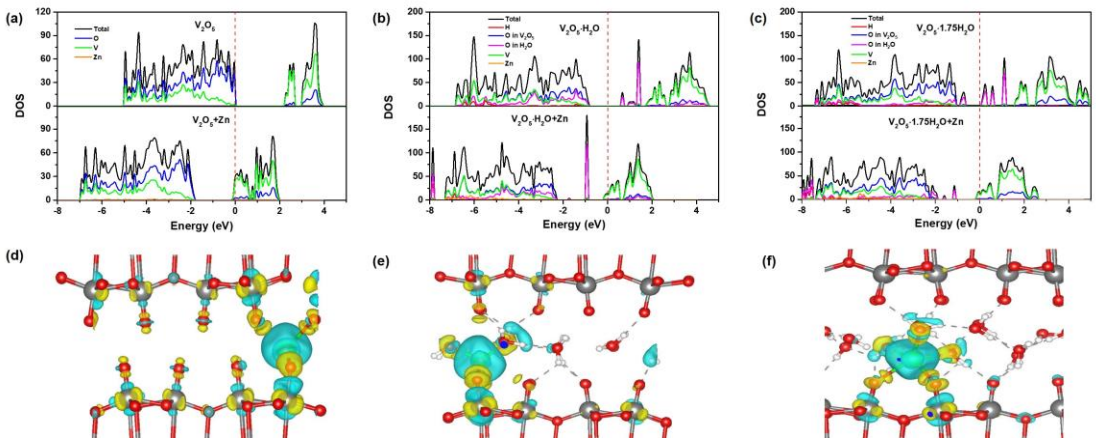

Fig. 4 The density of states for (a) V_2O_5 and V_2O_5+Zn, (b) $V_2O_5{\cdot}H_2O$ and $V_2O_5{\cdot}H_2O$+Zn, (c) $V_2O_5{\cdot}1.75H_2O$ and $V_2O_5{\cdot}1.75H_2O$+Zn. The red dash lines represent the location of Fermi level. The corresponding deformation charge density for V_2O_5, $V_2O_5{\cdot}H_2O$ and $V_2O_5{\cdot}1.75H_2O$ with Zn^{2+} intercalated are illustrated in (d), (e) and (f), respectively. The grey dash line stands for the hydrogen bond. The iso-surface of the deformation charge density is equal to 0.005 e/bohr^3.

To clarify the charge transfer of Zn, we also calculated deformation charge density. The deformation charge density of pristine and Zn^{2+}-intercalated structures are illustrated in Fig. 4d-f. The positive (in yellow) and negative (in blue) regions correspond to enrichment and depletion of electron density, respectively. There is an obvious charge transfer occurred between Zn and two V_2O_5-layers in the bilayer dry V_2O_5. The Zn loses lots of its electrons (corresponding to the large blue region) while the nearby V and O together receive electrons from Zn (corresponding to the yellow region). However, with the introduction of H_2O, charge transfer not only occurs between Zn and the bottom V_2O_5-layer, but also takes place between Zn and H_2O. Although the direction of electron transfer can be clearly obtained from deformation charge density, the quantitative number of electron transfer are still unknown, especially for similar blue region around Zn in the three structures illustrated.

Table 2 The average Bader charge (e) of O, V and Zn for different structures.

Compound	O	V	Zn
V_2O_5	-0.77	+1.92	/
V_2O_5+Zn	-0.78	+1.87	+1.33
$V_2O_5 \cdot H_2O$	-0.87	+1.91	/
$V_2O_5 \cdot H_2O$+Zn	-0.92	+1.90	+1.38
$V_2O_5 \cdot 1.75H_2O$	-0.96	+1.92	/
$V_2O_5 \cdot 1.75H_2O$+Zn	-1.00	+1.91	+1.39

To quantitatively describe the number of electrons transferred from Zn, Bader charge analysis was performed for O, V and Zn. The average Bader charge of O, V and Zn for different structures are listed in Table 2. The Bader charge of Zn-ions is +1.33*e* in dry-V_2O_5+Zn, and electrons from Zn decrease the average Bader charge of O and V when compared to pristine dry-V_2O_5. For V in dry-V_2O_5+Zn, the average Bader charge decreases from +1.92*e* to +1.87*e*, indicating V of variable oxidation- states contributes more to receive electrons from Zn. For $V_2O_5 \cdot H_2O$+Zn and $V_2O_5 \cdot 1.75H_2O$+Zn, the Bader charge of Zn increases to +1.38*e* and +1.39*e* when compared to dry-V_2O_5+Zn. This means Zn loses more electrons in the presence of water. The more electrons transferred the deeper the conduction band drops below the Fermi level as shown in Fig. 4b and 4c; it further leads to a higher formation energy between Zn and V_2O_5, which can also explain why the OCV is higher in $V_2O_5 \cdot H_2O$ and $V_2O_5 \cdot 1.75H_2O$ than dry-V_2O_5. Like dry-V_2O_5, the average Bader charge of V also decreases in $V_2O_5 \cdot H_2O$ and $V_2O_5 \cdot 1.75H_2O$ when Zn^{2+} is intercalated, but the degree of decrease is less than in dry-V_2O_5. The electrons in Zn^{2+}-intercalated hydrated V_2O_5 are mainly transferred into O, which causes the average Bader charge of O to decrease from -0.87e to -0.92e in $V_2O_5 \cdot H_2O$ and from -0.96e to -1.00e in $V_2O_5 \cdot 1.75H_2O$. It should be noted that O-ions with decreased Bader charge are mainly those in H_2O and in V_2O_5-sheet near Zn. This observation is consistent with our previous analysis of deformation charge density.

Zn^{2+}-Diffusion Pathway

The preceding section unveiled that the structural water influences thermodynamic properties of V_2O_5-based cathodes. However, thermodynamics is a necessary, but insufficient criterion to describe kinetic properties of a cathode material. An optimal cathode material must also be able to allow a fast diffusion of Zn^{2+}. Thus, Zn^{2+}-diffusion barriers in dry-V_2O_5, $V_2O_5{\cdot}H_2O$ and $V_2O_5{\cdot}1.75H_2O$ have been evaluated by the CI-NEB approach. Herein, two Zn^{2+} migration pathways along (010) and (110) directions are considered for the bilayer dry-V_2O_5, whereas we only consider one migration pathway along (010) direction for $V_2O_5{\cdot}H_2O$ and $V_2O_5{\cdot}1.75H_2O$ because of the strong steric effect of water along (110) direction, making Zn^{2+} difficult to diffuse along this direction. The migration pathways for all the structures investigated are shown in Fig. 5a-d, while Fig. 5e compares Zn^{2+} migration energies for dry-V_2O_5, $V_2O_5{\cdot}H_2O$ and $V_2O_5{\cdot}1.75H_2O$. In the case of dry-V_2O_5, Zn^{2+} diffusion barrier along (100) direction is 1.40 eV, which is slightly larger than that along (110) direction. This result indicates that Zn^{2+} prefers to diffuse along (110) direction in absence of water. On the other hand, diffusion barriers for Zn^{2+} in $V_2O_5{\cdot}H_2O$ and $V_2O_5{\cdot}1.75H_2O$ are only 0.66 eV and 0.81 eV, respectively, much lower than that for dry-V_2O_5, which suggests that the structural water in V_2O_5 acts as a "lubricant" to promote the diffusion of Zn^{2+}. A similar result was also obtained by Yan M. et al. in experiment and this "lubricant" effect was through to derive from the reduced "effective charge" of Zn by water-shielding.[30] However, except for the water "charge shielding" effect, our thermodynamic calculations above also suggest that O in H_2O can also act as extra host sites for Zn^{2+}, introducing the new charge interaction mechanism. Therefore, it may be insufficient to interpret the Zn diffusion in $V_2O_5{\cdot}H_2O$ and $V_2O_5{\cdot}1.75H_2O$ only by "charge shielding" effect.

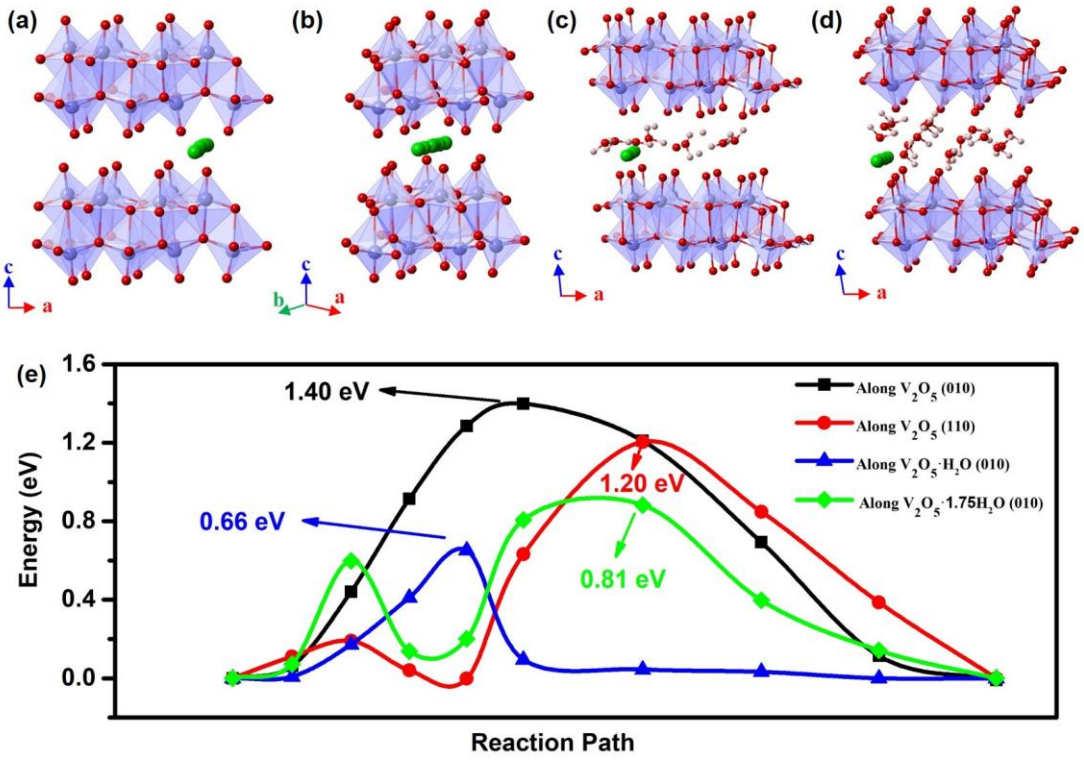

Fig. 5 Zn^{2+} migration pathways along (a) V_2O_5 (010) and (b) V_2O_5 (110), (c) $V_2O_5 \cdot H_2O$ (010) and (d) $V_2O_5 \cdot H_2O$ (110). (e) Zn^{2+} diffusion barriers for V_2O_5, $V_2O_5 \cdot H_2O$ and $V_2O_5 \cdot 1.75H_2O$

To understand the combined "charge shielding" and "O in H_2O interaction with Zn^{2+}" effect on Zn^{2+} diffusion, cross-sectional views of three-dimensional electrostatic potentials in dry-V_2O_5, $V_2O_5 \cdot H_2O$ and $V_2O_5 \cdot 1.75H_2O$ are calculated and shown in Fig. 6. The electrostatic potential environment for the three compounds is very similar. However, it is still observable that the electrostatic potential change along Zn^{2+} migration pathway (010) is smaller in $V_2O_5 \cdot H_2O$ and $V_2O_5 \cdot 1.75H_2O$ than in dry-V_2O_5. The result suggests that the structural water can help rebuild a smooth electrostatic environment within the gallery and reduce Zn^{2+} diffusion barriers along (010). Due to the small difference in Zn^{2+} diffusion barriers along (010) and (110) directions, the difference of electrostatic potential change along both directions is also small, making it hard to discern in the figure.

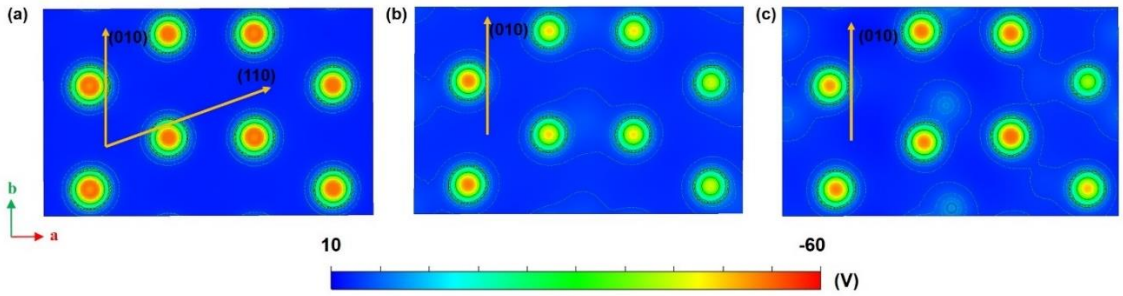

Fig. 6 The cross-sectional views of electrostatic potential for (a) V_2O_5, (b) $V_2O_5{\cdot}H_2O$ and (c) $V_2O_5{\cdot}1.75H_2O$. Zn^{2+} migration pathways are also indicated by orange arrows. The blue region represents positive potential and the red region represents negative potential. The iso-surface of the electrostatic potential equals to 7 V. It should be noted that the slice is an *a-b* plane cut out from the adsorbed Zn^{2+} sites.

Theoretical Specific Capacity

We further predict the theoretical specific capacity of dry-V_2O_5, $V_2O_5{\cdot}H_2O$ and $V_2O_5{\cdot}1.75H_2O$ in storing Zn^{2+} with the following expression:

$$C = \frac{1}{M}(x_{max} \nu F \cdot 10^3) \quad (3)$$

where M is the molecular weight of cathode formula unit, x_{max} is the maximum Zn^{2+} concentration that can be stored in cathode formula unit. According to the preceding section, x_{max} equals to 1.0, 0.5 and 1.0 for V_2O_5, $V_2O_5{\cdot}H_2O$ and $V_2O_5{\cdot}1.75H_2O$, respectively; $\nu = 2$ is the valence electron of Zn; F is Faraday's constant (26.801 Ah/mol). The calculated theoretical specific capacities are 294.52, 134.00 and 251.06 mAh/g for bilayer dry-V_2O_5, $V_2O_5{\cdot}H_2O$ and $V_2O_5{\cdot}1.75H_2O$, respectively. It is worth noting that bilayer dry-V_2O_5 has the highest specific capacity among the three materials because of its low molecular weight. The theoretical specific capacity of $V_2O_5{\cdot}1.75H_2O$ is lower than the experimental 381 mAh/g. We here speculate two possible reasons for this behavior. First, the non-faradaic contribution from the electrical double-

layer capacity effect (a physical process) is included in the experimental value, whereas the theoretical specific capacity calculation only considers Faradaic contribution; Second, the structural water in $V_2O_5 \cdot 1.75H_2O$ can exchange with Zn^{2+} reversibly, which makes the maximum Zn concentration in $V_2O_5 \cdot 1.75H_2O$ greater than 1. For this case, it can be verified by calculating the formation energy of exchange reaction between the structural water and Zn^{2+}. We add one more Zn^{2+} into $V_2O_5 \cdot 1.75H_2O$ containing eight Zn^{2+}, and exchange with one H_2O molecule:

$$Zn + Zn_8V_{16}O_{40} \cdot 14H_2O \rightarrow Zn_9V_{16}O_{40} \cdot 13H_2O + H_2O \quad (4)$$

The calculated Gibbs free energy change for this reaction is negative (−0.7 eV), which means that Zn^{2+} could thermodynamically replace a structural water in $V_2O_5 \cdot 1.75H_2O$ system.

Conclusions

In summary, the structural water effect on the crystal structure, intercalation voltage, migration barrier, capacity and electronic structures in bilayer dry-V_2O_5, $V_2O_5 \cdot H_2O$ and $V_2O_5 \cdot 1.75H_2O$ has been investigated using first-principle DFT calculations. The calculations indicate the structural water suited between two V_2O_5 sheets increases the gallery spacing. When Zn^{2+} are intercalated, these structural waters can shield charge interactions between Zn^{2+} and V_2O_5 sheets, thus decreasing the binding energy between Zn and V_2O_5. However, we also find O in H_2O can act as extra host sites to accept electrons from Zn, which is the fundamental reason for the increased OCV with H_2O. Furthermore, structural water can rebuild a smoother electrostatic environment under which a reduced diffusion barrier for Zn^{2+} diffusion is achieved. Last, we discuss the reasons of discrepancy between the theoretical and experimental specific capacity. In addition to the pseudocapacitive contribution in practical battery, the structural water in $V_2O_5 \cdot 1.75H_2O$

exchanging with Zn^{2+} is proposed as another reason. Overall, this work provides fundamental insights to the effect of structural water and Zn^{2+}-intercalation mechanisms in bilayer V_2O_5 system, which is expected to facilitate the design of new and better cathode materials for ZIBs.

Conflicts of interest

There are no conflicts to declare

Acknowledgments: This work is supported by National Science Foundation (NSF) under award NSF-DMR- 1464112.

Notes and references

1. N. Nitta, F. Wu, J. T. Lee and G. Yushin, *Mater. Today*, 2015, **18**, 252-264.

2. M. Tran, D. Banister, J. D. Bishop and M. D. McCulloch, *Nat. Clim. Chang.*, 2012, **2**, 328-333.

3. M. S. Whittingham, *Chem. Rev.*, 2004, **104**, 4271-4302.

4. J.-M. Tarascon and M. Armand, in *Materials For Sustainable Energy: A Collection of Peer-Reviewed Research and Review Articles from Nature Publishing Group*, World Scientific, 2011, 171-179.

5. E. P. Roth and C. J. Orendorff, *Electrochem. Soc. Interface*, 2012, **21**, 45-49.

6. T. C. Wanger, *Conserv. Lett.*, 2011, **4**, 202-206.

7. E. E. Evarts, *Nature*, 2015, **526**, S93-S95.

8. J. Ni, S. Fu, C. Wu, J. Maier, Y. Yu and L. Li, *Adv. Mater.*, 2016, **28**, 2259-2265.

9. S. Chen, C. Wu, L. Shen, C. Zhu, Y. Huang, K. Xi, J. Maier and Y. Yu, *Adv. Mater.*, 2017, **29**, 1700431.

10. J. C. Pramudita, D. Sehrawat, D. Goonetilleke and N. Sharma, *Adv. Energy Mater.*, 2017, **7**, 1602911.

11. G. Fang, J. Zhou, A. Pan and S. Liang, *ACS Energy Lett.*, 2018, **3**, 2480-2501.

12. H. Hou, C.E. Banks, M. Jing, Y. Zhang and X. Ji, *Adv. Mater.*, 2015, **27**, 7861-7866.

13. M. Winter and R. J. Brodd, *Chem. Rev*, 2004, **104**, 4245-4270.

14. Y. Wang, J. Yi and Y. Xia, *Adv. Energy Mater.*, 2012, **2**, 830-840.

15. W. Li, J. R. Dahn and D. S. Wainwright, *Science*, 1994, **264**, 1115-1118.

16. Y. Lu, J. B. Goodenough and Y. Kim, *J. Am. Chem. Soc.*, 2011, **133**, 5756-5759.

17. J.-Y. Luo, W.-J. Cui, P. He and Y.-Y. Xia, *Nat. Chem.*, 2010, **2**, 760-765.

18. M. Pasta, C. D. Wessells, R. A. Huggins and Y. Cui, *Nat. Commun.*, 2012, **3**, 1149.

19. Y. Liu, Y. Qiao, W. Zhang, H. Xu, Z. Li, Y. Shen, L. Yuan, X. Hu, X. Dai and Y. Huang, *Nano Energy*, 2014, **5**, 97-104.

20. X. Wu, Y. Luo, M. Sun, J. Qian, Y. Cao, X. Ai and H. Yang, *Nano Energy*, 2015, **13**, 117-123.

21. H. Zhang, K. Ye, K. Zhu, R. Cang, J. Yan, K. Cheng, G. Wang and D. Cao, *Chem.-Eur. J.*, 2017, **23**, 17118-17126.

22. A. Ponrouch, C. Frontera, F. Bardé and M. R. Palacín, *Nat. Mater.*, 2016, **15**, 169.

23. C. Xu, B. Li, H. Du and F. Kang, *Angew. Chem.*, 2012, **124**, 957-959.

24. D. Kundu, S. H. Vajargah, L. Wan, B. Adams, D. Prendergast and L. F. Nazar, *Energ. Environ. Sci.*, 2018, **11**, 881-892.

25. X. G. Zhang, *Corrosion and electrochemistry of zinc*, Springer Science & Business Media, 2013.

26. W. Sun, F. Wang, S. Y. Hou, C. Y. Yang, X. L. Fan, Z. H. Ma, T. Gao, F. D. Han, R. Z. Hu, M. Zhu and C. S. Wang, *J. Am. Chem. Soc.*, 2017, **139**, 9775-9778.

27. C. Xu, J. Liao, C. Yang, R. Z. Wang, D. Wu, P. C. Zou, Z. Y. Lin, B. H. Li, F. Y. Kang and C. P. Wong, *Nano Energy*, 2016, **30**, 900-908.

28. N. Zhang, F. Y. Cheng, J. X. Liu, L. B. Wang, X. H. Long, X. S. Liu, F. J. Li and J. Chen, *Nat. Commun.*, 2017, **8**, 9.

29. D. Kundu, B. D. Adams, V. Duffort, S. H. Vajargah and L. F. Nazar, *Nat. Energy* 2016, **1**, 16119.

30. M. Yan, P. He, Y. Chen, S. Wang, Q. Wei, K. Zhao, X. Xu, Q. An, Y. Shuang and Y. Shao, *Adv. Mater.*, 2018, **30**, 1703725.

31. P. Novak and J. Desilvestro, *J. Electrochem. Soc.*, 1993, **140**, 140-144.

32. E. Levi, Y. Gofer and D. Aurbach, *Chem. Mater.*, 2009, **22**, 860-868.

33. J. Song, M. Noked, E. Gillette, J. Duay, G. Rubloff and S. B. Lee, *Phys. Chem. Chem. Phys.*, 2015, **17**, 5256-5264.

34. K. W. Nam, S. Kim, S. Lee, M. Salama, I. Shterenberg, Y. Gofer, J. S. Kim, E. Yang, C. S. Park, J. S. Kim, S. S. Lee, W. S. Chang, S. G. Doo, Y. N. Jo, Y. Jung, D. Aurbach and J. W. Choi, *Nano Lett.*, 2015, **15**, 4071-4079.

35. G. Kresse and J. Furthmüller, *Phys. Rev. B*, 1996, **54**, 11169-11186.

36. G. Kresse and J. Hafner, *Phys. Rev. B*, 1994, **49**, 14251-14269.

37. G. Kresse and J. Hafner, *Phys. Rev. B*, 1993, **47**, 558-561.

38. G. Kresse and D. Joubert, *Phys. Rev. B*, 1999, **59**, 1758-1775.

39. P. E. Blöchl, *Phys. Rev. B*, 1994, **50**, 17953-17979.

40. V. I. Anisimov, F. Aryasetiawan and A. Lichtenstein, *J. Phys. Condens. Matter*, 1997, **9**, 767-808.

41. S. Grimme, *J. Comput. Chem.*, 2006, **27**, 1787-1799.

42. G. Henkelman, B. P. Uberuaga and H. Jónsson, *J. Chem. Phys.*, 2000, **113**, 9901-9904.

43. M. Liu, Z. Q. Rong, R. Malik, P. Canepa, A. Jain, G. Ceder and K. A. Persson, *Energ. Environ. Sci.*, 2015, **8**, 964-974.

44. Z. Rong, R. Malik, P. Canepa, G. Sai Gautam, M. Liu, A. Jain, K. Persson and G. Ceder, *Chem. Mater.*, 2015, **27**, 6016-6021.

45. H. H. Kristoffersen and H. Metiu, *J. Phys. Chem. C*, 2016, **120**, 3986-3992.

46. V. Petkov, P. N. Trikalitis, E. S. Bozin, S. J. Billinge, T. Vogt and M. G. Kanatzidis, *J. Am. Chem. Soc.*, 2002, **124**, 10157-10162.

47. J. Livage, P. Barboux, J. Badot and N. Baffier, *MRS Online Proceedings Library Archive*, 1988, **121**.

48. A. Parija, D. Prendergast and S. Banerjee, *ACS Appl. Mater. Inter.*, 2017, **9**, 23756-23765.

49. F. Wang, J. Yi, Y. Wang, C. Wang, J. Wang and Y. Xia, *Adv. Energ. Mater.*, 2014, **4**, 1300600.

50. E. M. Gavilán-Arriazu, O. A. Pinto, B. L. de Mishima, D. E. Barraco, O. A. Oviedo and E. P. M. Leiva, *Electrochem. Commun.*, 2018, **93**, 133-137.

51. G. Schmuelling, T. Placke, R. Kloepsch, O. Fromm, H. W. Meyer, S. Passerini and M. Winter, *J. Power Sources*, 2013, **239**, 563-571.

52. M. A. Sk and S. Manzhos, *J. Power Sources*, 2016, **324**, 572-581.

53. P. E. Pearce, A. J. Perez, G. Rousse, M. Saubanere, D. Batuk, D. Foix, E. McCalla, A. M. Abakumov, G. Van Tendeloo, M. L. Doublet and J. M. Tarascon, *Nat. Mater.*, 2017, **16**, 580-587.

TOC:

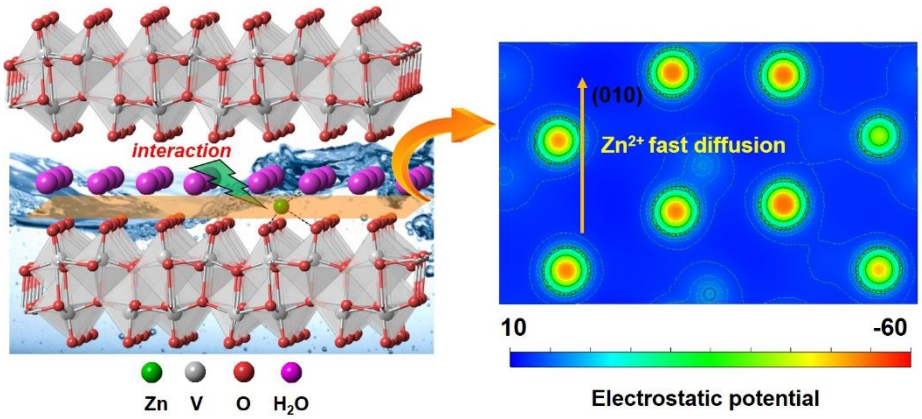
interaction
Zn
V
O
H2O
(010)
Zn2+ fast diffusion
10
-60
Electrostatic potential